PROTEINS
STRUCTURE ■ FUNCTION ■ BIOINFORMATICS

R248Q mutation—Beyond p53-DNA binding

Jeremy W. K. Ng,[1,2] Dilraj Lama,[2] Suryani Lukman,[2,3] David P. Lane,[4] Chandra S. Verma,[1,2,5] and Adelene Y. L. Sim[2]*

[1] Department of Biological Sciences, National University of Singapore, Singapore, Republic of Singapore
[2] Bioinformatics Institute, Agency for Science, Technology, and Research, Singapore, Republic of Singapore
[3] Department of Applied Mathematics and Sciences, Khalifa University of Science, Technology, and Research, Abu Dhabi, UAE
[4] p53 Laboratory, Agency for Science, Technology, and Research, Singapore, Republic of Singapore
[5] School of Biological Sciences, Nanyang Technological University, Singapore, Republic of Singapore

ABSTRACT

R248 in the DNA binding domain (DBD) of p53 interacts directly with the minor groove of DNA. Earlier nuclear magnetic resonance (NMR) studies indicated that the R248Q mutation resulted in conformation changes in parts of DBD far from the mutation site. However, how information propagates from the mutation site to the rest of the DBD is still not well understood. We performed a series of all-atom molecular dynamics (MD) simulations to dissect sterics and charge effects of R248 on p53-DBD conformation: (i) wild-type p53 DBD; (ii) p53 DBD with an electrically neutral arginine side-chain; (iii) p53 DBD with R248A; (iv) p53 DBD with R248W; and (v) p53 DBD with R248Q. Our results agree well with experimental observations of global conformational changes induced by the R248Q mutation. Our simulations suggest that both charge- and sterics are important in the dynamics of the loop (L3) where the mutation resides. We show that helix 2 (H2) dynamics is altered as a result of a change in the hydrogen bonding partner of D281. In turn, neighboring L1 dynamics is altered: in mutants, L1 predominantly adopts the recessed conformation and is unable to interact with the major groove of DNA. We focused our attention the R248Q mutant that is commonly found in a wide range of cancer and observed changes at the zinc-binding pocket that might account for the dominant negative effects of R248Q. Furthermore, in our simulations, the S6/S7 turn was more frequently solvent exposed in R248Q, suggesting that there is a greater tendency of R248Q to partially unfold and possibly lead to an increased aggregation propensity. Finally, based on the observations made in our simulations, we propose strategies for the rescue of R248Q mutants.

Proteins 2015; 83:2240–2250.

Key words: DNA-binding domain; molecular dynamics; p53.

INTRODUCTION

p53, also called the "guardian of the genome",[1] is a transcription factor that mediates a wide range of responses to cellular stress.[2,3] It is also one of the most commonly mutated genes across a wide range of cancers.[4,5] The gene codes for a 393 amino acid protein consisting of five domains: transactivation domain (TAD; modulates p53 levels and also recruits transcriptional machinery), the proline rich region (PR; site of interactions with multiple proteins), the DNA binding domain (DBD; site of dimerization and binding to target DNA, and site of interactions with multiple proteins), the oligomerization domain (responsible for the tetramerization of p53), and the C-terminus domain (CTD; regulates transcription and also site of interactions with multiple proteins).[6] The DBD is of particular interest as it is the most commonly mutated part of p53,[7] with more than 90% of all observed p53 mutations occurring within this region.[8]

The DBD comprises of ten beta sheets (S1–S10), three large loops (L1–L3), and two helices (H1–H2) (Fig. 1).[9] Helix 1 (H1) is responsible for mediating inter-molecular contacts in the DBD homodimer; the loops and helix 2 (H2) are responsible for DNA binding, with loop 1 (L1) and H2 binding to the major grove of DNA while loops 2 and 3 (L2–L3) interact with the minor grove.[10] Most mutations in the DBD occur at "mutation hotspots"—a

Additional Supporting Information may be found in the online version of this article.

*Correspondence to: Adelene Y. L. Sim, Bioinformatics Institute, Agency for Science, Technology, and Research, 30 Biopolis Street, Matrix, #07-01, Singapore 138671. E-mail: adelenes@bii.a-star.edu.sg

Received 7 August 2015; Revised 22 September 2015; Accepted 29 September 2015
Published online 7 October 2015 in Wiley Online Library (wileyonlinelibrary.com). DOI: 10.1002/prot.24940

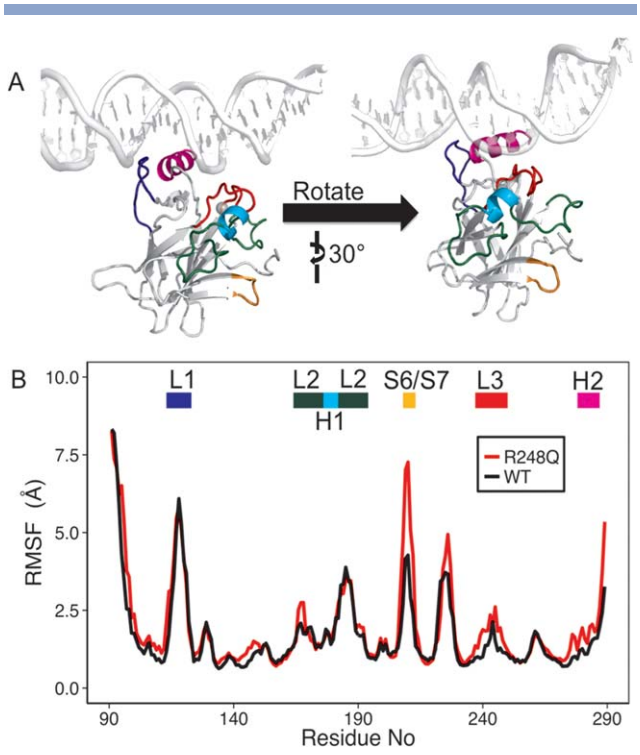

Figure 1

Structure of p53 DNA binding domain in its apo-state (PDBid 2XWR:A). (A) The DNA (white) is placed in its approximate binding location based on PDBid 3Q05. Important regions are highlighted: L1 (residues 113–123, blue), L2 (residues 164–176 and residues 177–181, green), L3 (residues 237–250, red), H1 (residues 177–181, cyan), H2 (residues 278–287, magenta), and S6/S7 (residues 208–213, orange). (B) Root mean squared fluctuation (RMSF) based on simulation data of the wild type (WT) and R248Q mutant are shown, with significant changes at L2, S6/S7, and L3 highlighted.

set of six residues (R175, G245, R248, R249, R273, and R282) that are mutated in more than 3% of all cancer cases.[5] Mutations are further categorized into either contact or structural mutants based on how they inactivate p53.[11] Contact mutants such as R248W, R248Q, and R273H are characterized by the loss of essential contacts of the DBD with the DNA leading to abrogation of DNA binding, yet without significant conformational changes in the DBD.[12] On the other hand, structural mutants such as R175H, G245S, R249S, and R282W exhibit extensive conformational changes in the DBD,[13] with a significant fraction of these structural mutants being unfolded under physiological conditions.[14]

R248 is a mutation hotspot, with mutations occurring in about 4% of all cancer patients.[15] From high-resolution crystal structure data,[16] the side-chain of R248 is observed to be solvent-exposed, and therefore not expected to directly participate in stabilizing the rest of the DBD. Additionally, R248 directly interacts with the minor grove of its target DNA. Thus, mutations to R248—usually R248A, R248W, and R248Q—have been widely considered as contact mutants.[17] In this study, we focus on the R248Q mutant, which is commonly observed in a wide range of human cancers such as colorectal cancer, lymphoid leukemia, and myeloid leukemia.[15]

Despite R248 appearing not to directly influence DBD stability and dynamics, experimental evidence suggests that R248Q mutant undergoes significant conformational changes. Nuclear magnetic resonance (NMR) experiments by Wong *et al.*[17] demonstrated that R248Q exhibits conformational changes throughout the DBD at L1, L2, L3, S2, S2', S4, S9, S10, and H2. The observed chemical shifts in R248Q are similar to those seen in R249S, a known structural mutant. Additionally, R248Q was found to be about 2 kcal/mol less stable compared with wild type p53 by comparing rates of urea-induced denaturation measured using fluorescence spectroscopy.[9,11] Recently, Xu *et al.* showed that the R248Q mutant is capable of aggregating with wild type p53 *in vitro*, suggesting the exposure of an otherwise buried hydrophobic patch from residues 252 to 257.[18] Taken together, these experimental observations suggest that the R248Q is also a structural mutant. Nonetheless, it remains unclear how information from the mutation site R248Q is propagated to influence the overall DBD conformation and stability.

We performed all-atom molecular dynamics (MD) simulations on the DBD to understand how mutations at R248 induce conformational changes in regions distant from the mutation site. In so doing, we attempt to elucidate the structural basis for the aforementioned experimental observations. p53 functions most efficiently as a tetramer, although it known to also exist in monomeric and dimeric forms *in vivo*.[19] As monomeric and tetrameric DBD are similar in their structural features [10,20,21] and thermodynamic stabilities,[22] most studies of the DBD are performed on monomers. Consequently, to minimize the computational complexity of our simulations, we also performed MD using monomeric forms of the DBD.

Because arginine has a long side-chain and an overall positive charge, mutations in R248 could influence DBD packing via electrostatic interactions and/or steric constraints, beyond interfering with the direct R248-DNA contact. We performed MD simulations on the wild type structure (WT) as well as on a series of mutants: R248 with an electrically neutral side-chain (R248RN), R248A, R248W, and R248Q. The R248RN simulations allow us to isolate the effect of arginine's charge, while the R248A and R248W simulations allow us to dissect the role of sterics in maintaining the DBD structure. Additionally, both R248A and R248W are common mutations that are observed in a wide range of cancers,[15] and studying them helps us to determine if a common mechanism exists to explain how R248A, R248Q, and R248W destabilize the DBD. However, the major focus of this article is on the R248Q mutant (Fig. 1); there also exists NMR chemical shift data on this mutant for comparison. After dissecting the mechanism(s) by which the R248Q mutant

Table I
Table Showing Simulations Performed, as well as Total Length of Simulation Time for Each Mutation. All Simulations were Performed in Triplicates

Mutation	Length (ns) per simulation	Total simulation time for analysis (ns)
WT	500	1,200
R248Q	500	1,200
R248A	200	300
R248RN	200	300
R248W	200	300

causes the DBD to undergo conformational changes, we propose some strategies for rescuing R248Q mutants.

METHODS AND MATERIALS

Molecular dynamics simulations

All simulations were started using chain A of the crystal structure 2XWR, comprising of residues 91 to 289 of p53 DBD.[23] The N- and C-termini of the protein were capped with C-acetyl and N-methyl caps respectively. Crystallographic waters were kept. Thereafter, the protein was solvated in a water box where the box edges are at least 10 Å away from the protein. Counter-ions (Na^+ or Cl^-) were added to ensure charge neutrality of the system. Mutations were performed using the *Pymol*[24] mutagenesis wizard.

Simulations were performed using the AMBER12 package[25] with the AMBER ff99SB force field.[26] (The neutral arginine charges were changed manually. All side-chain atomic charges were set to zero, while backbone charges were retained based on the AMBER ff99SB force-field. The charge on CB was manipulated to ensure overall neutrality of the residue.) Water was modeled using the TIP3P water model.[27] The tetrahedral coordinated zinc ion was modeled using a bonded zinc model, following parameters in Ref. 28. Hydrogen bond lengths were restrained using the SHAKE algorithm, allowing simulation time steps of 2 fs. Long-range electrostatics was treated with Particle Mesh Ewald (PME),[29] and a cut-off of 12 Å. Minimization was performed using 9500 cycles of conjugate gradient after minimization with steepest descent for 500 cycles. Thereafter, the system was heated up to 310K prior to the production run. We performed three independent simulations of 500 ns for WT and R248Q. Only the last 400 ns of each simulation was considered for analysis, yielding a total of 1.2 μs of simulation time for the WT and R248Q, respectively, for analysis. For R248A, R248W, and R248RN, the same protocol was used but only 200 ns of simulations were performed, of which only the last 100 ns of each simulation was considered for analysis. The simulations performed are summarized in Table I below. The root mean squared deviation (RMSD) of the backbone carbons across different trajectory are shown in Supporting Figure S7.

Additionally, a set of simulations were performed using the same protocol but with a temperature of 293K. Table II below shows the lengths of simulations performed for each mutant.

Conformational clustering and identification of S6/S7 states

In order to cluster structures into either having either 'exposed' or 'buried' S6/S7 turn, we calculated the distance between the backbone carbons of R207 and D259. Thereafter, we used *k-means* clustering to assign the membership of conformation to either being 'exposed' or buried'.

Structural analysis

Analysis was performed using the *cpptraj* module from AMBERTools 14[30] and *Bio3D*[31] from the R statistical software.[32] The trajectories were visualized using VMD,[33] while crystal structures were visualized using *Pymol*.[24]

Mutinf calculations

The backbone dihedral angles (phi and psi), as well as the side-chain angle (chi_1) angle was extracted from individual trajectories using the *g_chi* command in the Gromacs suite of analysis software.[34] Thereafter, the trajectories of WT and R248Q were split into three runs of 400 ns each prior, and provided as input for calculation of mutual information and KL-divergence using the Mutinf software.[35]

RESULTS AND DISCUSSION

Dynamics of the mutation-carrying loop L3

R248 resides in L3 (Fig. 1) which is less compact in the different mutants compared to the WT (based on radius of gyration, R_g, see Fig. 2(A)). This reduced packing of L3 is consistent with large-scale conformational changes observed via NMR in the L3 loop of the R248Q mutant.[17] Interestingly, the increased R_g was observed even in the R248RN and R248W simulations, suggesting that the charges and the size of the arginine side-chain are likely crucial in preserving wild type L3 loop conformations. Additionally, in the case of R248RN, the R_g of L3 showed a bimodal distribution with peaks centered at

Table II
Table Showing Simulations Performed at 293K, as well as Total Length of Simulation Time for Each Mutation. All Simulations were Performed in Triplicates

Mutation	Length (ns) per simulation	Total simulation time for analysis (ns)
WT	200	300
R248Q	200	300
R248A	200	300
R248W	200	300

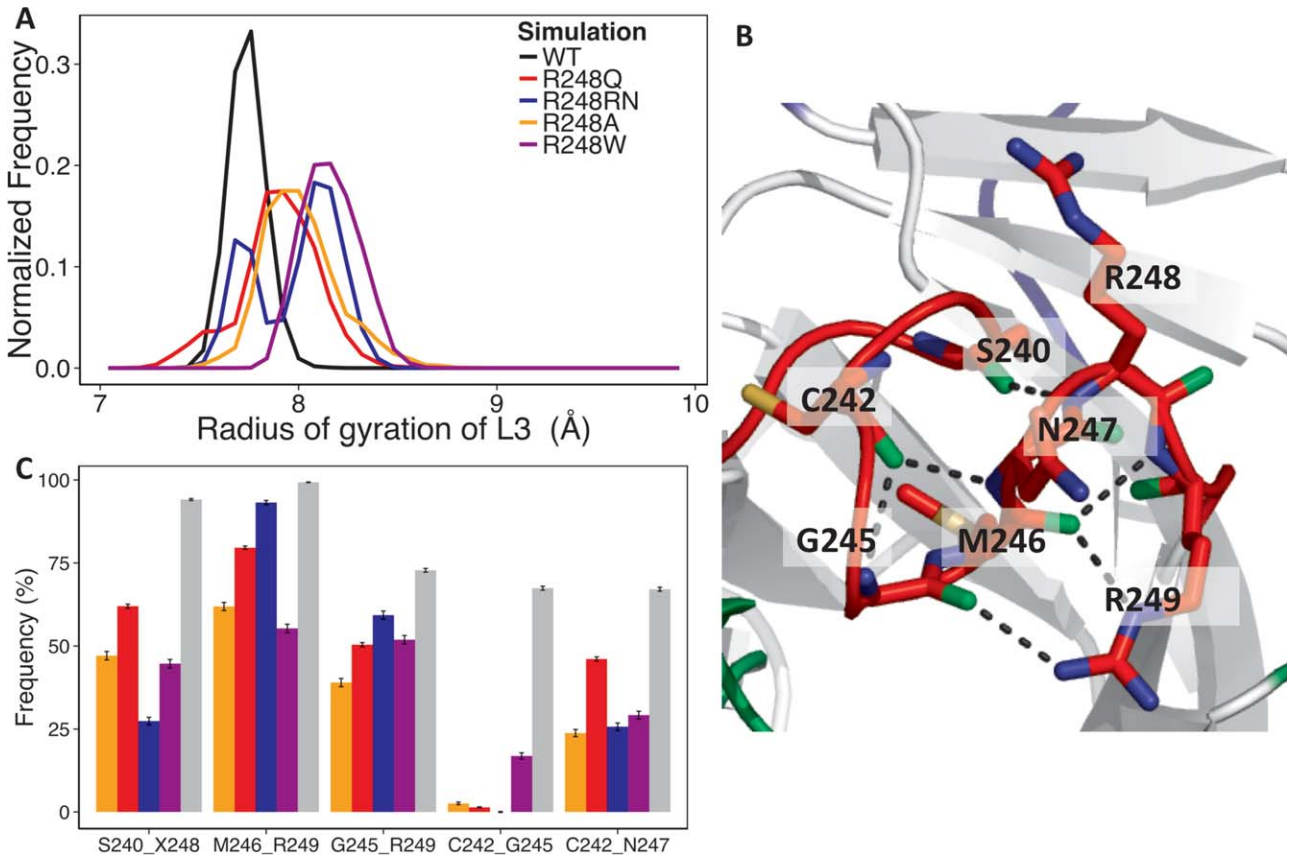

Figure 2

Conformational changes at loop L3 (M236-P250). (A) Radius of gyration of WT (black), R248RN (blue), R248Q (red), R248W (purple), and R248A (orange). WT L3 adopts a more compact structure compared with the mutants, while the radius of gyration of L3 shows a bimodal distribution in the case of R248RN. (B) Native hydrogen bonds observed in crystal structure (PDBid 2XWR:A) in the L3 loop. Oxygen atoms are colored green and nitrogen atoms in blue. (C) Bootstrapped frequency of native hydrogen bonds occurrence throughout the simulations of WT, R248RN, R248Q, and R248A. Most significant loss of hydrogen bonds observed in the simulations involves C242. [Color figure can be viewed in the online issue, which is available at wileyonlinelibrary.com.]

7.7 Å and 8.1 Å, while R_gs of R248Q and R248A appear to distribute between these two peaks. Inspection of the backbone dihedral angles shows that R_g is correlated with the backbone psi angle of G245 for R248RN (Supporting Figure S1), with the larger radius of gyration associated with a psi angle of about 0° (Supporting Figure S1). The dihedral angle of G245 drastically impacts the conformation of the L3 as G245 adopts a tight turn in the WT conformation;[21] consequently, a loss of this turn would cause the L3 to become less compact.

We expect that the hydrogen bond network of L3 would have a pronounced effect on L3 conformation. Hence, we identified key hydrogen bonds in L3 from our starting crystal structure (PDBid 2XWR:A) and monitored their frequencies throughout the simulations [Fig. 2(B,C)]. Figure 2(C) shows the frequency of several key hydrogen-bond interactions observed by bootstrapping. Noticeably, these interactions were lost or markedly less frequent in all the mutant simulations compared to WT, suggesting a rearrangement of hydrogen bond network when R248 is mutated. In particular, the C242–G245 interaction was lost in our mutant simulations. This hydrogen bond is critical in stabilizing G245's unique combination of backbone angles,[21] and occurs with high frequency in our WT simulations. The loss of this critical interaction could explain the loss of L3 packing observed in the mutants, as changes in backbone dihedrals around G245 alters the loop turn, causing L3 to become less compact. This is consistent with the observation that R_g correlates with the backbone angle of G245. Likewise, the observed loss of the S240-A/Q/RN248 interaction is consistent with earlier MD studies,[36] although the contribution of this loss of interaction to the destabilization of the DBD remains unclear.

Since the R248RN residue differs from the wild type arginine only in charge, the differences seen in Figure 2 suggest that the charge of R248 is crucial in maintaining the wild type L3 conformation. Conversely, R248RN and R248A have the same charge of zero, but differ in the size of their side chains, indicating that the size of the

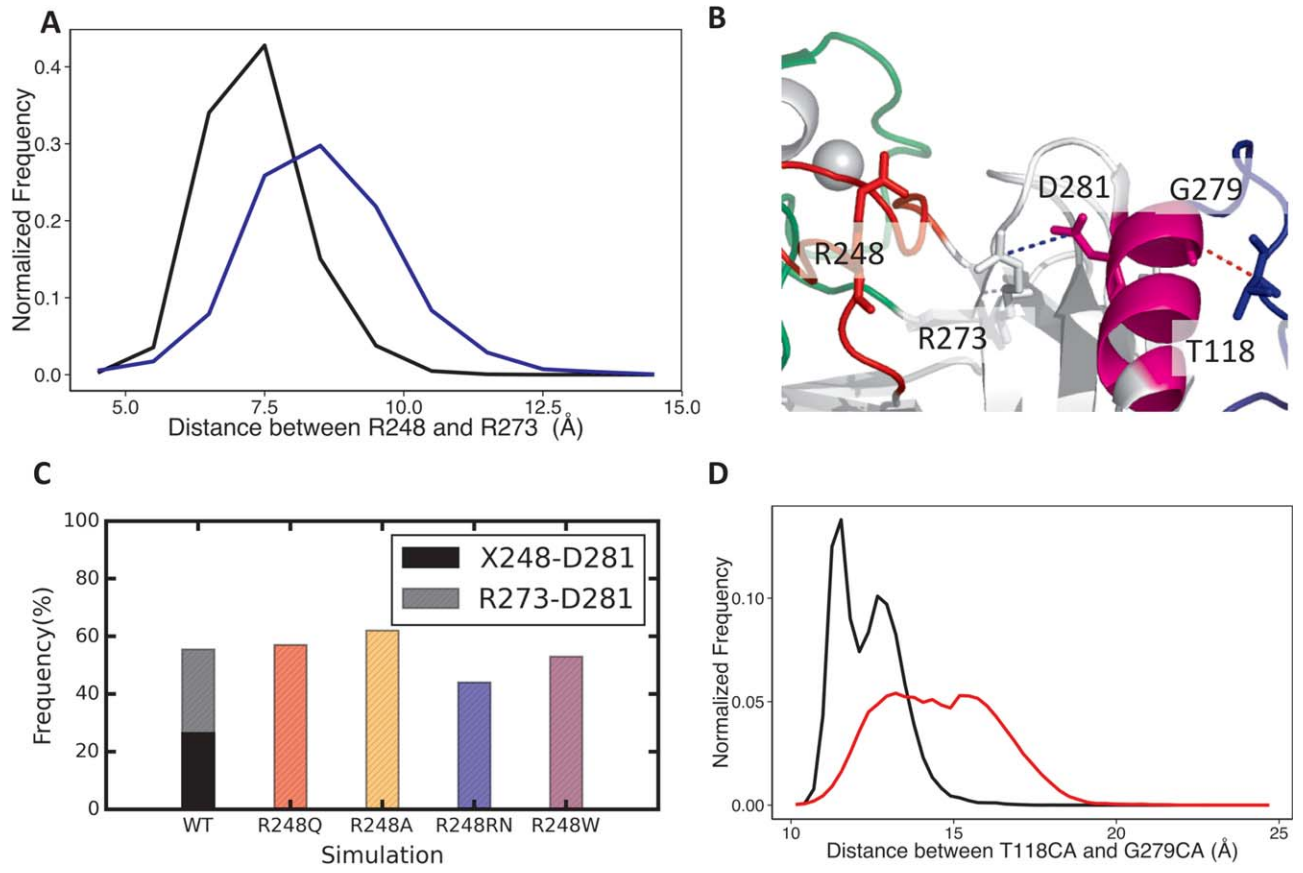

Figure 3

(A) Distance between CZs of R248 and R273 in WT (black) and R248RN (blue). Contrary to expectations based on the like-charge repulsion hypothesis, we noticed that R248RN had larger distances between the two terminal carbons of R248 and R273. (B) Crystal structure showing alternate interaction between R273 and D281 (blue dashed line). This interaction forms more frequently in mutant simulations (C). (D) As D281 on H2 interacts more frequently with R273, there was an increase in distance between the backbone carbons of T118 in L1 and G279 in H2, as shown in Figure 3(B) (red dashed line). This is further discussed in Figure 4. [Color figure can be viewed in the online issue, which is available at wileyonlinelibrary.com.]

size chain at residue 248 is also important in determining the packing of L3. Lastly, both R248W mutant and R248RN have large and neutral side chains, resulting in similar L3 R_g [Fig. 2(A)]. Taken together, both the charge and size of R248 appear to be instrumental in stabilizing the wild type L3 conformation. In particular, the L3 conformation is different for R248Q, R248A, and R248W (based on R_g and hydrogen bond distributions)—the three common mutants of R248 in p53. These differences will likely manifest in other aspects of DBD dynamics, as we discuss later below. We next examine the consequences of the altered dynamics of L3 on the neighboring regions.

Change in D281 interaction partner alters H2 and L1 dynamics

An earlier MD study by Merabet *et al.* suggested that when positively charged R248 is mutated to polar but uncharged Q, the loss of like-charge repulsion between R248 and R273 causes H2 (residues 278–287) to swing toward the central beta sheets (the core of p53) due to the increased flexibility of L3.[37] We measured the distance (CZ–CZ) between the side chains of residues R248 and R273 for the WT and R248RN, expecting either a decrease or no change in distances for the R248RN simulations because RN248 is electrically neutral and would not repel R273. However, contrary to the like-charge repulsion hypothesis, we observed that the average distance between R248RN and R273 was actually larger than the distance between R248 and R273 in WT [Fig. 3(A)]. We noticed that R248 was able to form hydrogen bonds with D281 [Fig. 3(C)] in WT. This interaction is lost in the uncharged RN248 and D281 is stabilized by interactions with spatially contiguous R273 more frequently in the R248RN simulations (also observed for other mutations; see Fig. 3(C)); that is there is a switch in the hydrogen bond partner of D281 from residue 248

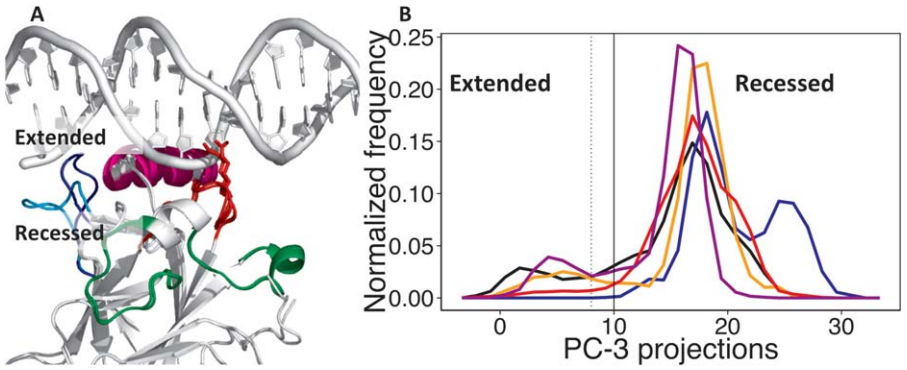

Figure 4

Dynamics of the L1 region of the p53 DBD. (A) The L1 loop adopts two conformations: the extended state (blue; from 3Q05) and the recessed state (cyan; from 2XWR). For reference, the bound DNA (from 3Q05) is also shown. (B) Projection of MD trajectories from WT (black), R248RN (blue), R248Q (red), and R248A (orange) onto the third principal component (PC3) identified in Ref. 38. PC3 was shown to separate the two conformations of L1. PC3 projections of < 10 were judged to be structures with an extended state, while PC3 projections >10 were recessed. Consistent with visual examination, recessed conformation appears most dominant; however, the extended state was sampled more often in the WT (19% versus 5%) than in R248Q. When a more stringent cut-off of eight (dashed line) is used, the dominance of the recessed conformations in the mutant simulations is more apparent. [Color figure can be viewed in the online issue, which is available at wileyonlinelibrary.com.]

to R273 that causes the H2 helix to move toward the core of the DBD. Our results from the R248RN simulations clearly contrast with the charge-repulsion hypothesis presented in Ref. 37. Our differing observations could be due to the choice of different force fields (GROMOS96/SPC water model versus AMBER ff99SB/TIP3P water model in our simulations) and sampling statistics (200ps equilibration and 10 ns production versus 100 ns equilibration and 100–400 ns production run in our simulations).

In crystal structures, H2 is shown to interact with L1 (residues 113–123). We thus expect that changes in H2 resulting as a consequence of the increased interactions between H2 and R273 on the S10 strand, will affect L1 conformation and/or dynamics. When visualizing the trajectories, we observed a loss of packing between H2 and L1 in the mutants. This is seen in a noticeable increase in distance between G279 and T118 in the R248Q mutant [Fig. 3(D); also for other mutants, as shown in Supporting Figure S2].

Recessed L1 conformation dominates mutant ensemble

The L1 loop adopts either an extended or a recessed conformation[38] [Fig. 4(A)] in crystal structures, with the extended conformation being favored when the DBD is bound to DNA[38] as L1 directly contacts the DNA via K120. Visual inspection of our trajectories suggests that in all our apo mutant and WT simulations, L1 is flexible and alternates between the extended and recessed states. We hypothesized that L1 should preferentially adopt the extended conformation in the WT simulations as compared to the mutants since the extended conformation is competent for DNA-binding. We used principal component analysis (PCA) to quantify the changes in the relative populations of recessed and extended conformations of L1 that are induced by the R248 mutations. From available crystallographic data, Lukman *et al.*[38] identified a set of principal components (PC) that distinguishes the two L1 conformations (PC 3 in Ref. 38). We projected our trajectories onto their identified PCs to quantify differences in L1 loop dynamics in both WT and the mutant simulations (R248A, R248RN, R248Q, and R248W). The results are shown in Figure 4(B).

Lukman *et al.* identified conformations with PC3 projection < 15 as being in the extended L1 conformation.[38] However, based on our density distributions, using PC3 projection < 10 as our threshold appears to be more appropriate due to the continuous nature of our data as juxtaposed to the discretized data from Lukman *et al.*[38] [Fig. 4(B)]. Consistent with our hypothesis, the WT explores extended conformations 19% of the time, but only 5% of the time in the R248Q mutant [Fig. 5(B)]; when a more stringent threshold of < 8 was considered, the WT samples the extended conformation 15% of the time while the R248Q samples it only 3% of the time. Similar to observations made in the R248Q mutant, both R248A and R248RN sample the extended conformation less extensively (0% in R248RN, 3% in R248A, using a threshold of 10). Most strikingly, R248RN does not sample the extended state, indicating a role of side-chain charge in R248 in determining the conformation of L1. This suggests that there is either an increase in the stability of the recessed L1, or a decrease in the stability of the extended L1 (or both) as compared to WT. As highlighted earlier, this can be attributed to the loss of hydrogen bond formation between RN248 and D281, and the accompanying increase in interactions between R273 and

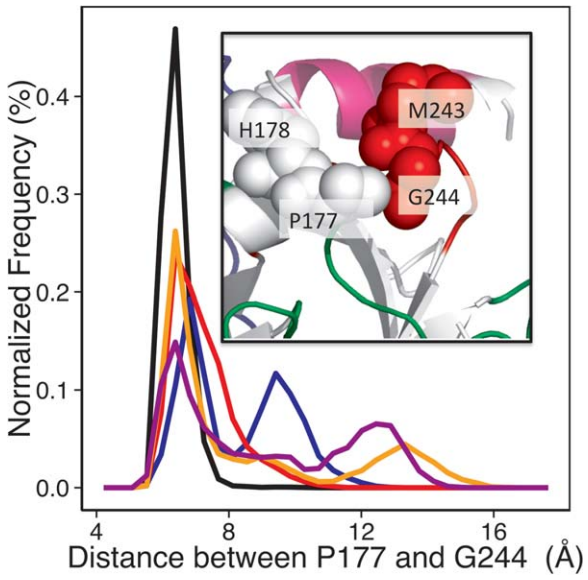

Figure 5

Distance between the backbone carbon of P177 and G244 (inset: P177 (white) and G244 (red) in sphere representation alongside adjacent residues to show spatial constraint) in WT (black), R248RN (blue), R248Q (red), R248W (purple), and R248A (orange). There are fewer spatial constraints exerted on P177 by G244 in the mutants, as the L3 loop is rearranged. As a result, P177- G244 distances increased in all the mutants. [Color figure can be viewed in the online issue, which is available at wileyonlinelibrary.com.]

D281. As a result of the change in hydrogen bonding network, H2 would be reoriented differently, causing a change in the packing of L1. However, R248W L1 samples the extended conformation almost as extensively as the WT (18.7% in R248W vs. 19% in WT) although hydrogen bonds were formed extensively throughout the simulation between R273 and D281, suggesting that the effects—and hence subsequently the rescue strategy—for R248W is mechanistically different from R248Q/A. Further studies in the R248W mutation are ongoing, and will be discussed elsewhere.

L1 interacts with the major groove of DNA at K120.[36] Consequently, changes in L1 dynamics unsurprisingly have a profound impact on the DNA-binding function of the DBD. Furthermore, Noskov *et al.* demonstrated that the binding of DNA by L1 is crucial in the stability of the DBD, underscoring the importance of L1 dynamics.[36] Our findings that L1 populates the extended and recessed states in both WT and R248Q is consistent with the conformational selection theory suggested in Ref. 39, where all possible conformations of a protein exist a priori, and the equilibrium distribution of states is shifted by a binding partner (DNA for example) "selecting" one state (in this case, the extended conformation of L1). In our simulations, the extended conformation is less populated in mutants, suggesting that DNA is less likely to conformationally select this state for binding. As a corollary, increasing the relative population of the extended state should enable us to recover interactions of the L1 loop with DNA. The importance of L1 dynamics in DBD function is further underscored by experimental studies by Merabet *et al.* where they showed that a second site mutation H115N is able to restore the DNA-binding activity of R248Q mutants by rigidifying L1.[37] They also find that rigidifying L1 via the second site mutation does not rescue R248W activity. These observations again suggest that the rescue strategy for R248Q (elaborated in this article) will likely be different from that for R248W.

Additionally, mutations at R248 often display perceptible temperature dependency. Temperature sensitive mutant R248W was shown to be able to bind DNA at sub-physiological temperatures.[40] R248A and R248Q were also found to be stable at sub-physiological temperatures.[13,17] We performed a series of additional simulations (see the Methods and Materials section) to study the effect of temperature on L1 dynamics. Consistent with our expectation, L1 sampled the extended conformation more extensively at sub-physiological temperatures than it did at physiological temperatures (Table III) in all the mutants except R248W.

Changes in dynamics of L2 when L3 rearranges

The alternative packing of L3 (where the mutations reside) has been shown for R248Q by NMR (at 10°C; Wong *et al.*[17]) to be associated with the rearrangement of L2 (residues 164–176 and 182–194). In the WT L3 configuration, G244 (on L3) is packed against P177 (on L2) as shown in Figure 5 (inset), leading to the rigidification of L2.[41] However, when the L3 loop undergoes rearrangements as in the case of all the mutants studied here, this packing constraint is released and G244 is no longer tightly packed with P177 (Fig. 5), thus resulting in increased flexibility in L2. For example, increased root mean squared fluctuations (RMSF) of the L2 loop around P177 can be seen in the R248Q mutant (Fig. 1). This however was not observed for the other mutants (see Supporting Figure S3), suggesting that the re-orientation of the L3 loop alone does not necessarily lead to increased L2 flexibility.

Mutual information can be used to identify concerted movements between regions, allowing us to identify allostery.[42] Then, the Kullback-Leiber (KL) divergence is

Table III

Percentages of Extended State L1 in Mutants at 293K and 310K

Simulation	293K	310K
WT	92.1	19.1
R248Q	95.1	5.0
R248A	91.0	14.3
R248W	18.4	18.8

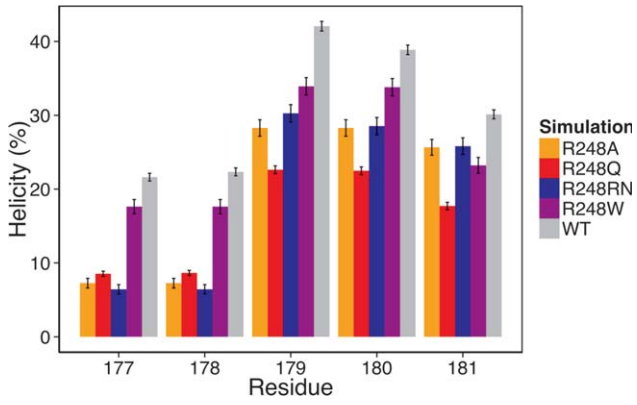

Figure 6

Percentage of helicity around the H1 region (residues 177 to 181) for the various trajectories, from 1000 bootstraps. Consistent with visual inspection, helicity was lost in all the mutants as compared to the WT (black). [Color figure can be viewed in the online issue, which is available at wileyonlinelibrary.com.]

used as a measure to compare the difference in mutual information. We evaluated the KL divergence between dihedrals of R248Q and WT (backbone and side-chain χ_1 angles) to quantify differences between their structural ensembles.[43] In our simulations, we observed that KL-divergence between WT and R248Q appears most concentrated at the zinc-coordination interface (Supporting Figure S4) between L2 and L3. This zinc interface is crucial in modulating L2 and L3 dynamics as it tethers the two loops together. Changes in the zinc interface could thus lead to a decoupling of L2 from L3, leading to an increase in flexibility of the L2 loop as observed in Figure 1.

Another significant difference that we visually observed between the WT and the R248Q mutant is the loss of the helicity in H1. To quantify our observation, we performed 1000 bootstraps using the Monte Carlo algorithm to reconstitute the structural ensemble, and then identifying the structures that possessed helical secondary structures. Noticeably, helicity is lost in not only the R248Q mutant, but also all the other mutants (Fig. 6). Earlier work by Duan *et al.*[44] suggested the role of a zinc coordinating residue, H179, in maintaining the structure of the H1 helix. In our simulations, we also observed a change in the side-chain dihedral of H179 (WT $\chi \sim -70^{o}$, R248Q $\chi \sim -55^{o}$), confirming that a re-orientation of the zinc binding interface likely underlies the large scale conformational changes in L2 observed in NMR experiments from Wong *et al.*[17]

Changes around the zinc binding interface also serves as a possible model for the dominant negative effect of the R248Q mutation observed in Ref. 18. The loss of zinc can lead to increased aggregation of DBDs, as is observed in R175H.[14] A limitation of our simulations is the choice using a bonded zinc model that covalently binds zinc to the coordinating residue. (This is necessary to keep the correct tetrahedral coordination of zinc.) As a result, zinc could not dissociate during our simulations. Despite this, our observation of H179 re-arrangement and H1 unfolding is also consistent with other simulation work using a non-bonded zinc model.[44]

Taken together, our data suggests that the NMR chemical shifts observed at the L2 region of the R248Q mutant[17] could likely arise as a result of two mechanisms associated with the re-arrangement of loop L3: (i) the re-arrangement of L3 relieves spatial constraints imposed by the tight packing of G244 (in L3) and P177 (in L2) present in WT and (ii) the zinc interface is reconfigured by the reorientation of H179 (in L2) and the unfolding of H1 (H1 is flanked by L2). These two changes lead to the increased flexibility observed in the L2 loop in the R248Q mutant. Finally, in our simulations, the L2–L3 packing and H1 helicity are also distinct for R248W compared to the other mutants, again highlighting a fundamental difference between the R248W and R248Q/A mutations.

Increased flexibility in S6/S7 turn not observed in previous NMR studies

All our mutant simulations showed increased flexibility at the S6/S7 turn (Fig. 1). Visual inspection of the trajectories reveals that the S6/S7 turn takes two distinct conformations –exposed and buried [Fig. 7(A)]. These conformational changes are potentially important in identification of intermediate conformations between the WT and the denatured conformations of the DBD. S7 contains the epitope-binding site of the antibody Pab240[17]—an antibody that is known to be specific for denatured p53.[45]

We clustered the conformations based on the state of the S6/S7 turn (see the Materials and Methods section). A total of 21% of the WT population was identified as being in the exposed state, as compared with 33% of the population being exposed in the R248Q mutant. From the starting crystal structure (PDBid 2XWR), we identified a hydrogen bond between the backbone carbonyl of M169 and the side-chain guanidinium of R213 (S6/S7 turn) that was lost in the mutants [Fig. 7(B,C)], leading to the exposure of the S6/S7 turn in the mutants.

Although the changes around the S6/S7 turn are prominent in our simulations, NMR data from Ref. 17 did not show changes in the chemical shifts between WT and R248Q. A possible reason could be the difference in temperatures used in the two studies: Wong *et al.*,[17] carried out the NMR measurements at sub-physiological temperatures (293K), hence stabilizing the protein in its folded states, while our simulations were carried out at 310K (body temperature). It is known that at 310K, the rate of unfolding of the protein increases even for WT p53.[46] In order to confirm if the change in S6/S7 dynamics were indeed due to differences in temperatures, we performed additional simulations at 293K. We observed no differences in RMSF between WT and the

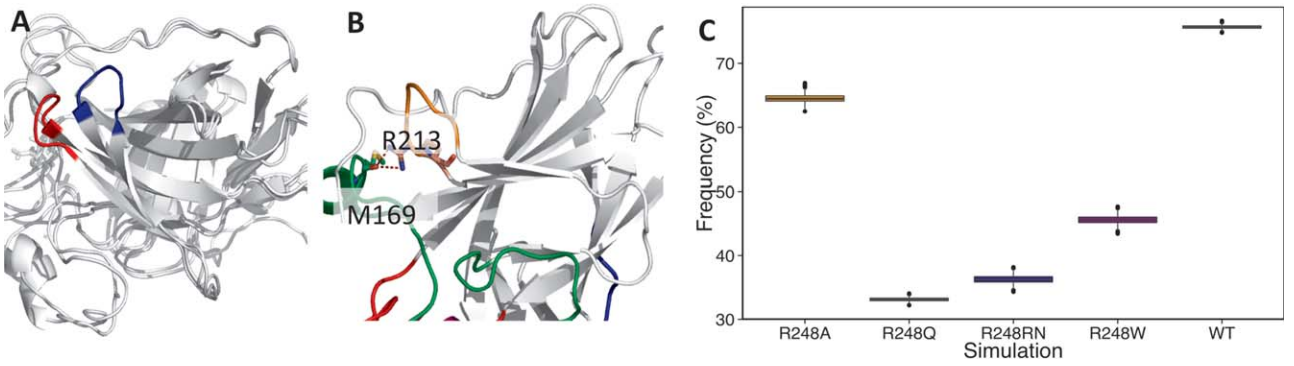

Figure 7

Changes at the S6/S7 turn. (A) The S6/S7 turn adopts two states: one that is exposed (red) and one that is buried (blue). (B) This M169-R213 interaction bridges the S6/S7 turn (orange) to the L2 loop (green). (C) The hydrogen bond interaction between the L2 and S6/S7 turn between M169 and R213 was reduced in all the mutants studied. [Color figure can be viewed in the online issue, which is available at wileyonlinelibrary.com.]

other mutants (except R248W) at 293K (Supporting Figure S5), providing direct evidence that DBD dynamics is influenced by temperature.

The dynamics of the S6/S7 turn is important because of its role in epitope recognition by antibodies. Antibodies are used extensively to identify conformations of p53 DBD. Ory *et al.* showed that Pab240 (that recognizes residues on the S7 strand) does not bind to R248Q mutants, suggesting that the S7 strand is unexposed in R248Q.[12] Instead, they showed that R248Q mutants, like WT, bind to Pab1620, an antibody that recognizes residues 145–157 spanning the S3 and S4 strands and residues 201–212 (S6/S7).[47] Taken together, these studies suggest that R248Q and WT have similar conformations in these regions. The experimental observation of Ory *et al.*[12] is consistent with our simulations: while the intervening loop between S6 and S7 (the S6/S7 turn) is exposed, the S6 and S7 strands remain only partially exposed, and therefore unable to bind to the Pab240 antibody. On the other hand, the epitope of Pab1620 remained exposed throughout our simulations. From our observations, the S6/S7 turn is a plausible novel epitope-binding site that can be used to recognize intermediate conformations between folded and unfolded DBD.

Strategies for rescuing R248Q mutants

Atomistic simulations such as the ones presented here offer us insights into the dynamics of mutant proteins, and provides us with possible clues into development of new therapeutic strategies. Based on our simulations, we suggest three strategies that could potentially rescue the R248Q mutant:

i. Rigidify L1, as demonstrated by Merabet *et al.*[37] By stabilizing L1 in the extended conformation, we likely will rescue of p53 DNA binding activity via the restoration of K120-DNA contact.[48] A possible candidate is the small molecule drug PRIMA-1, which was found to rescue the R175H mutant by binding a transient pocket located between L1 and S3, thereby stabilizing the L1 conformation.[49] Further work to probe whether the same pocket is exposed in R248Q using, for example, benzene-mapping[50] is needed to determine if PRIMA-1 would be effective in rescuing R248Q mutants.
ii. Maintain the zinc-binding pocket and hence the conformation of the L2–L3 interface. For example, the small molecule drug ZMC1 was shown to rescue R175H mutants by functioning as a zinc-metallochaperone.[51] Comparison between the dynamics of R175H mutant and R248Q mutant will help to elucidate if ZMC1 is appropriate for stabilizing zinc coordination in the R248Q mutant.
iii. Preserve H1 conformation to stabilize the L2 interface. Consequently, the stabilization of the L2 interface would stabilize other regions such as the L3 and the S6/S7 turn, which are directly tethered to this region (via hydrogen bonds/zinc coordination).

CONCLUSION

Although earlier experimental data suggest R248 is crucial in maintaining the structure of the DBD, understanding of why the solvent exposed R248 affects p53 stability is limited. To decipher how R248 is involved in stabilizing the DBD, we isolated the effects of sterics and charge on p53 DBD conformation using all-atom MD simulations of a series of mutations. We showed that: (i) both size and charge of R248 contribute to the conformation of L3, (ii) L3 influences H2 dynamics via changing H-bond partners of D281 on the H2, and (iii) as a result of changes in H2 dynamics, L1 predominantly adopts the recessed conformation in mutants. We focused on the R248Q mutant that is common in a

range of cancers and has been observed to exert a dominant negative effect. Our data suggest that the zinc ion that tethers L2 and L3 might dissociate more readily in the R248Q mutant due to changes at the L2 and L3 interface, hence facilitating the formation of aggregates as observed in experiments.[52]

The effects of the structural changes observed in our study could also potentially inhibit p53's ability to interact with other protein partners. Supporting Figure S6 summarizes the interactions (known and predicted[53]) that might be altered as a result of changes to p53 DBD induced by the R248Q mutation. The L2–L3 interface is an important protein-binding target and changes to the conformation at this interface would inevitably impact the binding ability of the DBD to other regulatory proteins such as 53BP1, 53BP2, and SV40 (Supporting Figure S6).

Finally, based on observations made from our R248Q simulations, we proposed a few possible strategies to rescue the function of R248Q mutant p53. Following up from this study, we are presently probing for cryptic binding pockets around L1 that can be exploited to rigidify L1 to the extended conformation. We are also studying the alternative mechanism by which R248W mutant causes a loss of DBD function.

ACKNOWLEDGMENT

We would like to thank the Verma lab for useful discussions.

REFERENCES

1. Lane D. Cancer. p53, guardian of the genome. Nature 1992;358;15–18.
2. Vogelstein B, Lane D, Levine A. Surfing the p53 network. Nature 2000;408;301–310.
3. Li T, Kon N, Jiang L, Tan M, Ludwig T, Zhao Y. Tumor suppression in the absence of p53-mediated cell-cycle arrest, apoptosis, and senescence. Cell 2012;149;1269–1283.
4. Nigro J, Baker S, Preisinger A. Mutations in the p53 gene occur in diverse human tumour types. Nature 1989;342;705–708.
5. Hollstein M, Sidransky D, Vogelstein B, Harris C. p53 mutations in human cancers. Science 1991;253;49–53.
6. Viadiu H. Molecular architecture of tumor suppressor p53. Curr Top Med Chem 2008;53;1327–1324.
7. Pavletich N, Chambers K, Pabo C. The DNA-binding domain of p53 contains the four conserved regions and the major mutation hot spots. Genes Dev 1993;7;2556–2564.
8. Olivier M, Eeles R, Hollstein M, Khan MA, Harris CC, Hainaut P. The IARC TP53 database: New online mutation analysis and recommendations to users. Hum Mutat 2002;19;607–614.
9. Bullock AN, Henckel J, DeDecker BS, Johnson CM, Nikolova P V, Proctor MR, Lane DP, Fersht AR. Thermodynamic stability of wild-type and mutant p53 core domain. Proc Natl Acad Sci USA 1997; 94;14338–14342.
10. Kitayner M, Rozenberg H, Kessler N, Rabinovich D, Shaulov L, Haran TE, Shakked Z. Structural Basis of DNA Recognition by p53 Tetramers. Mol Cell 2006;22;741–753.
11. Bullock A, Henckel J, Fersht A. Quantitative analysis of residual folding and DNA binding in mutant p53 core domain: definition of mutant states for rescue in cancer therapy. Oncogene 2000;19;1245–1256.
12. Ory K, Legros Y, Auguin C, Soussi T. Analysis of the most representative tumour-derived p53 mutants reveals that changes in protein conformation are not correlated with loss of transactivation or inhibition. Embo J 1994;13;3496–3504.
13. Barakat K, Issack B, Stepanova M, Tuszynski J. Effects of temperature on the p53-DNA binding interactions and their dynamical behavior: comparing the wild type to the R248Q mutant. PloS one 2011;6:e27651.
14. Butler JS, Loh SN. Structure, function, and aggregation of the zinc-free form of the p53 DNA binding domain. Biochemistry 2003;42; 2396–2403.
15. Petitjean A, Mathe E, Kato S, Ishioka C, Tavtigian SV, Hainaut P, Olivier M. Impact of mutant p53 functional properties on TP53 mutation patterns and tumor phenotype: Lessons from recent developments in the IARC TP53 database. Hum Mutat 2007;28;622–629.
16. Cho Y, Gorina S, Jeffrey P, Pavletich N. Crystal structure of a p53 tumor suppressor-DNA complex: understanding tumorigenic mutations. Science 1994;265:346–355.
17. Wong KB, DeDecker BS, Freund SM, Proctor MR, Bycroft M, Fersht AR. Hot-spot mutants of p53 core domain evince characteristic local structural changes. Proc Natl Acad Sci USA 1999;96;8438–8442.
18. Xu J, Reumers J, Couceiro JR, De Smet F, Gallardo R, Rudyak S, Cornelis A, Rozenski J, Zwolinska A, Marine J-C, Lambrechts D, Suh YA, Rousseau F, Schymkowitz J. Gain of function of mutant p53 by coaggregation with multiple tumor suppressors. Nat Chem Biol 2011;7;285–295.
19. Rajagopalan S, Huang F, Fersht AR. Single-molecule characterization of oligomerization kinetics and equilibria of the tumor suppressor p53. Nucleic Acids Res 2011;39;2294–2303.
20. Ho WC, Fitzgerald MX, Marmorstein R. Structure of the p53 core domain dimer bound to DNA. J Biol Chem 2006;281;20494–20502.
21. Wang Y, Rosengarth A, Luecke H. Structure of the human p53 core domain in the absence of DNA. Acta Crystallogr Sect D: Biol Crystallogr 2007;63;276–281.
22. Lubin DJ, Butler JS, Loh SN. Folding of Tetrameric p53: Oligomerization and Tumorigenic Mutations Induce Misfolding and Loss of Function. J Mol Bio 2010;395;705–716.
23. Natan E, Baloglu C, Pagel K, Freund SMV, Morgner N, Robinson CV, Fersht AR, Joerger AC. Interaction of the p53 DNA-binding domain with its N-terminal extension modulates the stability of the p53 tetramer. J Mol Biol 2011;409;358–368.
24. DeLano WL. The PyMOL Molecular Graphics System. Schrödinger LLC wwwpymolorg. 2002; Version 1.7.2.1. Available at: http://www.pymol.org.
25. Case DA, Berryman JT, Betz RM, Cerutti DS, Cheatham TE III, Darden TA, Duke RE, Giese TJ, Gohlke H, Goetz AW, Homeyer N, Izadi S, Janowski P, Kaus J, Kovalenko A, Lee TS, LeGrand S, Li P, Luchko T, Luo R, Madej B, Merz KM, Monard G, Needham P, Nguyen H, Nguyen HT, Omelyan I, Onufriev A, Roe DR, Roitberg A, Salomon-Ferrer R, Simmerling CL, Smith W, Swails J, Walker RC, Wang J, Wolf RM, Wu X, York DM, Kollman PA. AMBER 2015. University of California, San Francisco, 2015.
26. Hornak V, Abel R, Okur A, Strockbine B, Roitberg A, Simmerling C. Comparison of multiple amber force fields and development of improved protein backbone parameters. Proteins Struct Func Genet 2006;65;712–725.
27. Jorgensen WL, Chandrasekhar J, Madura JD, Impey RW, Klein ML. Comparison of simple potential functions for simulating liquid water. J Chem Phys 1983;79:926.
28. Madhumalar A, Smith DJ, Verma C. Stability of the core domain of p53: insights from computer simulations. BMC Bioinformatics 2008;9 Suppl 1:S17.
29. Darden T, York D, Pedersen L. Particle mesh Ewald: An N log(N) method for Ewald sums in large systems. J Chem Phys 1993;98: 10089.

30. Case DA, Darden T Iii TEC, Simmerling C, Brook S, Roitberg A, Wang J, Southwestern UT, Duke RE, Hill U, et al. AMBER 14. 2014.
31. Grant BJ, Rodrigues APC, ElSawy KM, McCammon JA, Caves LSD. Bio3d: an R package for the comparative analysis of protein structures. Bioinformatics 2006;22;2695–2696.
32. R Development Core Team R. R: A Language and Environment for Statistical Computing. R Found Stat Comput 2011;1:409.
33. Humphrey W, Dalke A, Schulten K. VMD: Visual molecular dynamics. J Mol Graph 1996;14;33–38.
34. Van Der Spoel D, Lindahl E, Hess B, Groenhof G, Mark AE, Berendsen HJC. GROMACS: Fast, flexible, and free. J Comput Chem 2005;26;1701–1718.
35. McClendon CL, Friedland G, Mobley DL, Amirkhani H, Jacobson MP. Quantifying correlations between allosteric sites in thermodynamic ensembles. J Chem Theory Comput 2009;5;2486–2502.
36. Noskov SY, Wright JD, Lim C. Long-Range Effects of Mutating R248 to Q/W in the p53 Core Domain. J Phy Chem B 2002;106; 13047–13057.
37. Merabet A, Houlleberghs H, Maclagan K, Akanho E, Bui TTT, Pagano B, Drake AF, Fraternali F, Nikolova PV. Mutants of the tumour suppressor p53 L1 loop as second-site suppressors for restoring DNA binding to oncogenic p53 mutations: structural and biochemical insights. Biochem J 2010;427;225–36.
38. Lukman S, Lane DP, Verma CS. Mapping the structural and dynamical features of multiple p53 DNA binding domains: insights into loop 1 intrinsic dynamics. PloS one 2013;8:e80221.
39. Kumar S, Ma B, Tsai CJ, Sinha N, Nussinov R. Folding and binding cascades: dynamic landscapes and population shifts. Protein Sci 2000;9;10–19.
40. Friedlander P, Legros Y, Soussi T, Prives C. Regulation of mutant p53 temperature-sensitive DNA binding. Journal of Biological Chemistry 1996;271;25468–25478.
41. Joerger AC, Ang HC, Fersht AR. Structural basis for understanding oncogenic p53 mutations and designing rescue drugs. Proc Natl Acad Sci USA 2006;103;15056–15061.
42. Lange OF, Grubmüller H. Generalized correlation for biomolecular dynamics. Proteins Struct Func Genet 2006;62;1053–1061.
43. McClendon CL, Hua L, Barreiro G, Jacobson MP. Comparing conformational ensembles Using the Kullback-Leibler divergence expansion. J Chem Theory Comput 2012;8;2115–2126.
44. Duan J, Nilsson L. Effect of Zn2+ on DNA recognition and stability of the p53 DNA-binding domain. Biochemistry 2006;45;7483–7492.
45. Gannon JV, Greaves R, Iggo R, Lane DP. Activating mutations in p53 produce a common conformational effect. A monoclonal antibody specific for the mutant form. Embo J 1990;9;1595–1602.
46. Butler JS, Loh SN. Folding and misfolding mechanisms of the p53 DNA binding domain at physiological temperature. Protein Sci 2006;15;2457–2465.
47. Wang PL, Sait F, Winter G. The "wildtype" conformation of p53: epitope mapping using hybrid proteins. Oncogene 2001;20;2318–2324.
48. Pan Y, Ma B, Venkataraghavan RB, Levine AJ, Nussinov R. In the quest for stable rescuing mutants of p53: Computational mutagenesis of flexible loop L1. Biochemistry 2005;44;1423–1432.
49. Wassman CD, Baronio R, Demir Ö, Wallentine BD, Chen C-K, Hall LV, Salehi F, Lin D-W, Chung BP, Hatfield GW, et al. Computational identification of a transiently open L1/S3 pocket for reactivation of mutant p53. Nature Commun 2013;4:1407.
50. Tan YS, Śledź P, Lang S, Stubbs CJ, Spring DR, Abell C, Best RB. Using ligand-mapping simulations to design a ligand selectively targeting a cryptic surface pocket of polo-like kinase 1. Angewandte Chemie - Int Ed 2012;51;10078–10081.
51. Yu X, Blanden AR, Narayanan S, Jayakumar L, Lubin D, Augeri D, Kimball SD, Loh SN, Darren R. Small molecule restoration of wild-type structure and function of mutant p53 using a novel zinc-metallochaperone based mechanism. Oncotargets 2014;5;8879–8892.
52. Ano Bom APD, Rangel LP, Costa DCF, De Oliveira GAP, Sanches D, Braga CA, Gava LM, Ramos CHI, Cepeda AOT, Stumbo AC, De Moura Gallo CV, Cordeiro Y, Silva JL. Mutant p53 aggregates into prion-like amyloid oligomers and fibrils: Implications for cancer. J Biol Chem 2012;287;28152–28162.
53. Tuncbag N, Kar G, Gursoy A, Keskin O, Nussinov R. Towards inferring time dimensionality in protein-protein interaction networks by integrating structures: the p53 example. Mol Biosyst 2009;5;1770–1778.